ADVANCES IN ATMOSPHERIC SCIENCES, VOL. 32, DECEMBER 2015, 1603–1616

Evaluation of CMIP5 Climate Models in Simulating 1979–2005 Oceanic Latent Heat Flux over the Pacific

CAO Ning[1], REN Baohua*[1], and ZHENG Jianqiu[1,2]

[1]*School of Earth and Space Sciences, University of Science and Technology of China, Hefei* 230026
[2]*Key Laboratory of Meteorological Disaster of Ministry of Education, Nanjing University of Information Science and Technology, Nanjing* 210044

(Received 20 January 2015; revised 25 May 2015; accepted 10 June 2015)

ABSTRACT

The climatological mean state, seasonal variation and long-term upward trend of 1979–2005 latent heat flux (LHF) in historical runs of 14 coupled general circulation models from CMIP5 (Coupled Model Intercomparison Project Phase 5) are evaluated against OAFlux (Objectively Analyzed air–sea Fluxes) data. Inter-model diversity of these models in simulating the annual mean climatological LHF is discussed. Results show that the models can capture the climatological LHF fairly well, but the amplitudes are generally overestimated. Model-simulated seasonal variations of LHF match well with observations with overestimated amplitudes. The possible origins of these biases are wind speed biases in the CMIP5 models. Inter-model diversity analysis shows that the overall stronger or weaker LHF over the tropical and subtropical Pacific region, and the meridional variability of LHF, are the two most notable diversities of the CMIP5 models. Regression analysis indicates that the inter-model diversity may come from the diversity of simulated SST and near-surface atmospheric specific humidity. Comparing the observed long-term upward trend, the trends of LHF and wind speed are largely underestimated, while trends of SST and air specific humidity are grossly overestimated, which may be the origins of the model biases in reproducing the trend of LHF.

Key words: model evaluation, climatology, trend, latent heat flux, CMIP5

Citation: Cao, N., B. H. Ren, and J. Q. Zheng, 2015: Evaluation of CMIP5 climate models in simulating 1979–2005 oceanic latent heat flux over the Pacific. *Adv. Atmos. Sci.*, **32**(12), 1603–1616, doi: 10.1007/s00376-015-5016-8.

1. Introduction

Earth's weather is driven largely by the behaviors of two large-scale atmospheric circulation systems: the Hadley circulation and Walker circulation. The ocean forms an important component of the climate system (Bigg et al., 2003) and is thought to be responsible for a significant amount of the heat transport (Trenberth and Solomon, 1994). Solar radiation absorbed by the ocean not only drives the movement of ocean water, but also provides energy to the atmosphere for driving atmospheric circulations by evaporation, long-wave radiation and sensible heat flux (Kiehl and Trenberth, 1997; Trenberth et al., 2009). These ocean–atmosphere interactions mainly occur in the tropics, and thus the changes of atmospheric circulation and ocean–atmosphere heat transport have been tied to variations of climate in most parts of the globe (Trenberth, 1995).

Ocean surface heat fluxes, including turbulence heat fluxes and radiation heat fluxes, are of great importance in measuring ocean–atmosphere heat and water exchange (Li et al., 2011b). An important mechanism of heat transport is water phase change, especially evaporation, which is the direct result of surface latent heat flux (LHF) and forms an important part of the hydrological cycle. The spatial and temporal variabilities of heat flux and the influence of atmospheric circulation on it have been explored in previous studies (Cayan, 1992a, 1992b, 1992c; O'Brien and Horsfall, 1995; Alexander and Scott, 1997; Yu et al., 2004; Papadopoulos et al., 2013), and the spatial patterns and temporal variability of LHF in the intraseasonal band have been characterized using satellite observations (Grodsky et al., 2009). State-of-the-art objective analysis approaches provide us with datasets that serve the needs of the ocean and climate research community, and bring us an objective view of annual, seasonal and interannual variability of air–sea heat fluxes (Yu and Weller, 2007; Yu et al., 2007).

Using bulk parameterization and similarity theory described by Liu et al. (1979), the surface LHF can be computed from the following relation:

$$\mathrm{LHF} = \rho L_\mathrm{e} C_\mathrm{e} U (q_\mathrm{s} - q_\mathrm{a}) = \rho L_\mathrm{e} C_\mathrm{e} U \Delta q \,, \qquad (1)$$

where q_s is the saturation specific humidity at the SST, q_a is the near-surface atmospheric specific humidity, Δq repre-

* Corresponding author: REN Baohua
Email: ren@ustc.edu.cn

sents the difference between q_s and q_a, U is the near-surface wind, ρ is the density of air, L_e is the latent heat of evaporation, and C_e is a turbulent exchange coefficient determined by the atmospheric stability, the air–sea temperature differences, and the wind. As q_s is a function of SST, the surface LHF can be determined from observable state variables of U, SST and q_a. As Earth warms in response to humans driving up levels of CO_2 by burning fossil fuels, the warming air and water will greatly change the mean state and variability of LHF. The Clausius–Clapeyron equation describes the water-holding capacity of the atmosphere as a function of temperature, and typical values are about 7% change for 1°C change in temperature. So, the specific humidity will change with the climate change (i.e., global warming).

How the thermal state of the western North Pacific warm pool influences surface LHF was discussed by Zhou (2013) and their associations with tropical cyclone genesis were investigated by Zhou et al. (2015). For longer time scales, Gulev (1995) explored the climatological variations of ocean–atmosphere heat transfer with respect to long-term climate changes in the North Atlantic, and the trend of surface heat flux has also been discussed in warming-related changes (Yu and Weller, 2007) and the dynamic part, i.e., wind circulation (Liu and Curry, 2006). Li et al. (2011a) investigated the long-term trend of ocean surface LHF over the tropical and subtropical Pacific (TSP) and suggested that the positive surface LHF trend was closely associated with both the warming forces (direct/local causes) and the surface wind circulation (indirect/nonlocal factor).

To uncover interpretations from the perspective of climate dynamics, coupled general circulation models (CGCMs), which are sophisticated tools designed to simulate the Earth's climate system and the complex interactions between its components (Reichler and Kim, 2008), are increasingly common in climate research. The Coupled Model Intercomparison Project (CMIP) began in 1995 under the auspices of the Working Group on Coupled Modelling, as part of the International Research Programme on Climate Variability and Predictability. Its purpose is to examine climate variability and predictability as simulated by the models, and to evaluate the model results against available observations, providing a community-based infrastructure in support of climate model diagnosis, validation, intercomparison, documentation and data access (Meehl et al., 1997, 2000). Scores of modeling studies have shown that increasing greenhouse gases in the atmosphere impact the global hydrological cycle (Zhou et al., 2011). Strengthening trends of the tropical atmospheric circulation have been shown in a number of previous studies, using both reanalysis data (Quan et al., 2004; Mitas and Clement, 2006; Burgman et al., 2008) and satellite observation data (Chen et al., 2002; Wentz et al., 2007). However, general circulation models simulating the influence of increased greenhouse gases produce a weakening of the tropical overturning circulation that affects the Walker circulation more strongly than the Hadley circulation (Held and Soden, 2006; Vecchi et al., 2006; Vecchi and Soden, 2007). Yulaeva et al. (2010) modeled the North Pacific climate variability forced by oceanic heat flux anomalies. So, exploring the changes of circulation and heat transport with global warming has been of great importance.

Given the fact that climate models feature a considerable margin of error in terms of tropical atmospheric circulations compared with observed and reanalysis data, achieving further understanding of how models simulate LHF, which is an important atmospheric circulation heat source, is emerging as a highly necessary avenue of research. In this paper, we evaluate 14 CMIP5 models based on their performances in simulating the climatological mean state, climatological seasonal variation and long-term trend of oceanic LHF, and discuss the possible origins of model biases. The inter-model diversity in simulating the mean fields of LHF is also discussed. The remainder of the paper is organized as follows: The data and method used in this study are described in section 2. The evaluation results and possible bias origins of the climatological mean state, inter-model diversity, climatological seasonal variation and long-term trend of surface LHF simulated in the CMIP5 historical runs against observations are presented in section 3. Finally, in section 4, a summary and discussion of the paper are provided.

2. Data and method

In this study, the climatological mean state, climatological seasonal variation and long-term trend of oceanic LHF simulated in the historical runs of CMIP5 climate models are evaluated against observations. The inter-model diversity of 14 CMIP5 CGCMs in simulating the annual mean climatological LHF is discussed. The model data come from the 20th century (20C3M) historical runs in the World Climate Research Programme (WCRP) CMIP5 multi-model dataset. The observed oceanic surface LHF data come from the Objectively Analyzed air–sea Fluxes (OAFlux) project at Woods Hole Oceanographic Institution. The OAFlux project aims to provide consistent, multi-decadal, global analyses of air–sea heat, evaporation, and momentum fluxes for use in studies of the global energy budget, water cycle, atmosphere and ocean circulation, and climate. The objective analysis approach takes into account data errors in the development of enhanced global flux fields. The flux-related variables in the OAFlux dataset are obtainable from three major sources: marine surface weather reports from voluntary observing ships, satellite remote sensing, and numerical weather prediction (NWP) reanalysis and operational analysis outputs (Yu et al., 2008).

To lend credence to the evaluation results, reliability analysis on the LHF in the OAFlux data is first performed using surface flux data from the National Oceanography Centre, Southampton, Version 2.0 (NOCS V2) surface flux and meteorological dataset. The NOCS V2 dataset is a monthly mean gridded dataset of marine surface measurements and derived fluxes constructed using optimal interpolation. Inputs for the period 1973 to 2006 are the International Comprehensive Ocean-Atmosphere Data Set (ICOADS) Release 2.4 ship data, and the update from 2007 to 2013 uses ICOADS Release 2.5. The dataset is presented as a time series of monthly

mean values on a 1° area grid. Because the OAFlux dataset and NOCS V2 dataset are derived from different data sources and algorithms, they have different sources of errors (Yu et al., 2008; Berry and Kent, 2009, 2011). They also differ from NWP model fluxes in that NWP-modeled surface meteorological variables are just part of the input datasets for the synthesis, and the OAFlux procedure uses the state-of-the-art Coupled Ocean–Atmosphere Response Experiment (COARE) 3.0 bulk flux algorithm (Fairall et al., 2003). So, using the NOCS V2 dataset to verify the reliability of the OAFlux dataset is reasonable.

We perform a *t*-test on the signal-to-noise ratio (SNR) defined as follows (Hayashi, 1982):

$$r_{\mathrm{H}} = \frac{\Delta\overline{x}}{\sigma(\Delta x)}\,, \tag{2}$$

where $\Delta\overline{x} = \overline{x}_2 - \overline{x}_1$ and $\Delta x = x_2 - x_1$. $\Delta\overline{x}$ is the climatological mean difference between the two datasets, and $\sigma(\Delta x)$ is the standard variance difference between the two datasets, reflecting the mean vibration condition of their difference. As is known, each climate state can be decomposed to the climatological mean state and biases as $x = \overline{x} + e$, and then $\Delta x = \Delta\overline{x} + \Delta e$, in which the mean state is constant. By performing an analysis of variance on this equation, we can obtain $\sigma^2(\Delta x) = \sigma^2(\Delta e)$, in which $\sigma(\Delta x)$ is the mean variance of difference between the two datasets, i.e., noise, and $\Delta\overline{x}$ is the signal. The ratio of them is the SNR of the climate state of these two datasets. Figure 1 shows the result of the *t*-test on the SNR of the annual mean and seasonal mean [DJF (December–January–February) and JJA (June–July–August) mean] LHF during 1979–2005 from the OAFlux and NOCS V2 datasets. The figure shows that, at the 90% confidence level, the LHF of the OAFlux dataset matches well with that of NOCS V2 for the annual mean and seasonal mean. There are regions in the subtropical Pacific not exceeding the 90% confidence level due to the lack of *in situ* data. However, the OAFlux data are combined with post-1985 satellite remote sensing state-variables data; so, for our study period (1979–2005), the OAFlux data are more credible. Given this, it is reliable to use the OAFlux data as observations in evaluating the models.

Correspondingly, the heat flux products are grouped into three categories: ship-based products, satellite-based products, and NWP reanalysis products (Yu et al., 2008). Combining different sources of data helps reduce systematic error. The OAFlux global products have demonstrated in many ways their value in stimulating advances in our understanding of the role of the ocean in the global energy budget, the global hydrological cycle, and the change and variability of the Earth's climate (Yu et al., 2008). In previous studies, the decadal change of global oceanic evaporation (proportional to LHF) is marked by a distinct transition from a downward trend to an upward trend around 1977–78 (Yu, 2007); and since this transition, global oceanic evaporation has been rising continuously. Thus, to evaluate the continuous trend of LHF, the study period should be after this transition. So, the starting year of this study is set to be 1979. The exact lengths

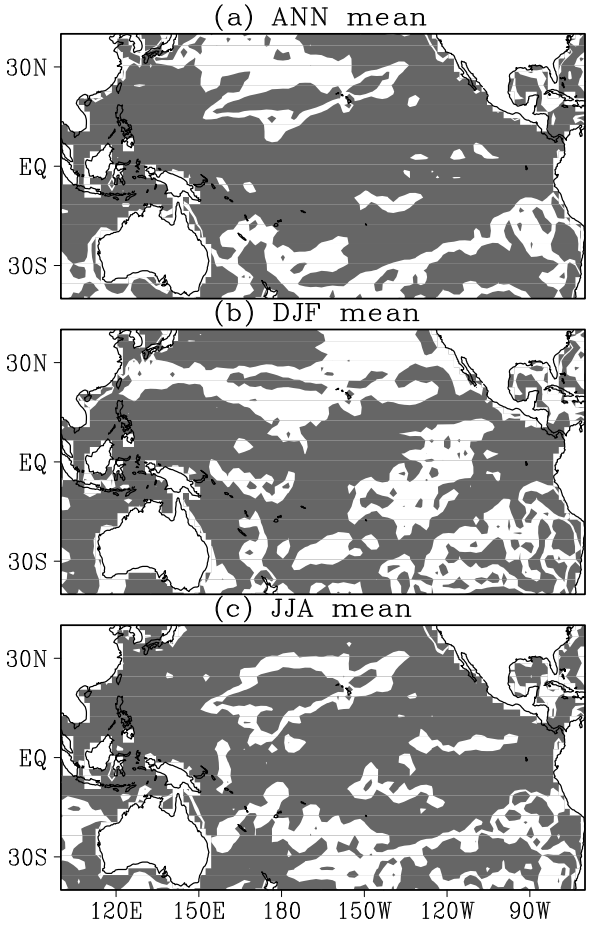

Fig. 1. Two-tailed Student's *t*-test on the SNR of the LHF differences between the OAFlux and NOCS V2 datasets for the (a) annual average, (b) northern winter average (DJF), and (c) austral winter average (JJA). The time period of the LHF data is 1979–2005. Shaded areas indicate the SNR exceeds the 90% confidence level.

of the models' outputs vary, but most of the models end their simulations at the year 2005. Therefore, the period 1979–2005 is designated as the time period of this study, with further studies on the climatological mean fields, seasonal variations and long-term trend. Information on the 14 models involved in this study including their modeling centers (or groups), institute IDs, model names, and output time periods of their 20C3M experiments, is presented in Table 1. The multi-model ensemble (MME) mean is calculated by mathematically averaging the 14 models' simulations. The air–sea heat interaction mainly occurs in the TSP, so the study domain is set to cover this region: (40°S–40°N, 100°E–70°W).

The resolutions of all the monthly fields of the model simulations and observations are re-gridded to 2° × 2° using the inverse distance weighting approach. All spatial averaging and correlation calculations use area weighting, where areas changing between meridians at varying latitudes are considered by using the cosine of the latitude as weights. Inter-model EOF analysis (Li and Xie, 2012) is used to validate

Table 1. Information on the 14 CMIP5 models involved in this study.

Modeling center or group	Institute ID	Model name	Historical run (YYYYMM)
Beijing Climate Center, China Meteorological Administration	BCC	BCC-CSM1.1	185001–201212
Canadian Centre for Climate Modelling and Analysis	CCCMA	CanESM2	185001–200512
Community Earth System Model Contributors	NSF-DOE-NCAR	CESM1-CAM5	185001–200512
Centre National de Recherches Météorologiques/Centre Européen de Recherche et Formation Avancée en Calcul Scientifique	CNRM-CERFACS	CNRM-CM5	185001–200512
Commonwealth Scientific and Industrial Research Organization in collaboration with Queensland Climate Change Centre of Excellence	CSIRO-QCCCE	CSIRO-Mk3.6.0	185001–200512
LASG, Institute of Atmospheric Physics, Chinese Academy of Sciences	LASG-IAP	FGOALS-s2	185001–200512
NOAA Geophysical Fluid Dynamics Laboratory	NOAA GFDL	GFDL-ESM2M	186101–200512
NASA Goddard Institute for Space Studies	NASA GISS	GISS-E2-R	185001–200512
Met Office Hadley Centre	MOHC	HadCM3	185901–200512
Institute for Numerical Mathematics	INM	INM-CM4	185001–200512
L'Institute Pierre-Simon Laplace	IPSL	IPSL-CM5A-LR	185001–200512
Japan Agency for Marine-Earth Science and Technology, Atmosphere and Ocean Research Institute (University of Tokyo), and National Institute for Environmental Studies	MIROC	MIROC-ESM	185001–200512
Meteorological Research Institute	MRI	MRI-CGCM3	185001–200512
Norwegian Climate Centre	NCC	NorESM1-M	185001–200512

the diversity of these models in simulating the climatology of LHF.

3. Results

The models simulate the oceanic LHF in their historical runs and the biases of these simulations are manifested in several aspects such as the climatological mean state, seasonal variations and long-term trend. The inter-model diversity of the 14 CMIP5 models in reproducing the annual mean climatological LHF is also discussed.

3.1. *Climatological mean state*

The annual mean (January–December) and seasonal mean (DJF and JJA) climatology of oceanic surface LHFs for the period 1979–2005 using model simulations and observations are computed first. The spatial distributions of the simulated mean state (no single model is shown in this paper, but the MME mean distributions for the annual mean, DJF mean and JJA mean are shown in Figs. 2a, c and e) show that all 14 models can generally reproduce the spatial pattern of observed annual and seasonal mean LHF climatology (Figs. 2b, d and f, using OAFlux data), although there are some significant biases in simulated amplitudes. Overestimations are found throughout the models, but there are regional variations that can be captured. Comparing the MME mean LHF climatology of the annual mean in Fig. 2a with that of the OAFlux data in Fig. 2b, the major features match well. The agreement in terms of the strong and weak latent heat release centers is very good. The strong latent heat release centers fall in regions such as the Pacific western boundary current (including the Kuroshio Current and its extension, which is strongest in boreal winter; and the East Australian Current and its extension, which is strongest in boreal summer), the tropical Pacific alongside the equator, the Gulf Stream, and equatorward northwest region off the Australian west coast. The weak latent heat release centers mainly fall in the Pacific "cold tongue" region and 30° latitude (south and north) poleward Pacific regions. Although the models can capture the mean fields of LHF fairly well, there are overestimations both in strong and weak latent heat release regions, which means the models simulate stronger LHF over most of the TSP. The differences between the CMIP5 outputs and OAFlux can be as large as 20–30 W m^{-2} in the subtropical oceans according to the MME mean. These results can be further verified by comparing the seasonal mean (DJF in Figs. 2c, d and JJA in Figs. 2e, f) climatology of the MME and OAFlux data.

To quantitatively evaluate the models' performances, the Taylor diagram (Taylor, 2001), which can provide a visual framework for comparing model simulation results to observations, is used. Figure 3 graphically summarizes how closely the spatial pattern of the annual mean, DJF mean and JJA mean climatology of LHF, and related state variables such as near-surface wind speed, SST and near-surface atmospheric specific humidity, obtained from the models' outputs, match the observations of the OAFlux data. The radial distance from the origin represents the fraction of the modeled spatial variation pattern that can be explained by the observed (OAFlux) spatial pattern. The spatial correlation coefficient between the model output and observation is denoted by the angular distance from the *x*-axis. The centered root-mean-square error (RMSE) between the simulated and observed patterns is proportional to the distance to the point on the *x*-axis identified as "OBS". Models simulating patterns of climatology that agree well with observations will lie nearest the "OBS" point. These models will have relatively high correlation and low RMSEs. Models lying on the boldface dashed arc will have the correct standard deviation, which indicates that the pattern variations are of the right amplitude.

In Fig. 3a, for the annual mean climatology, the pattern

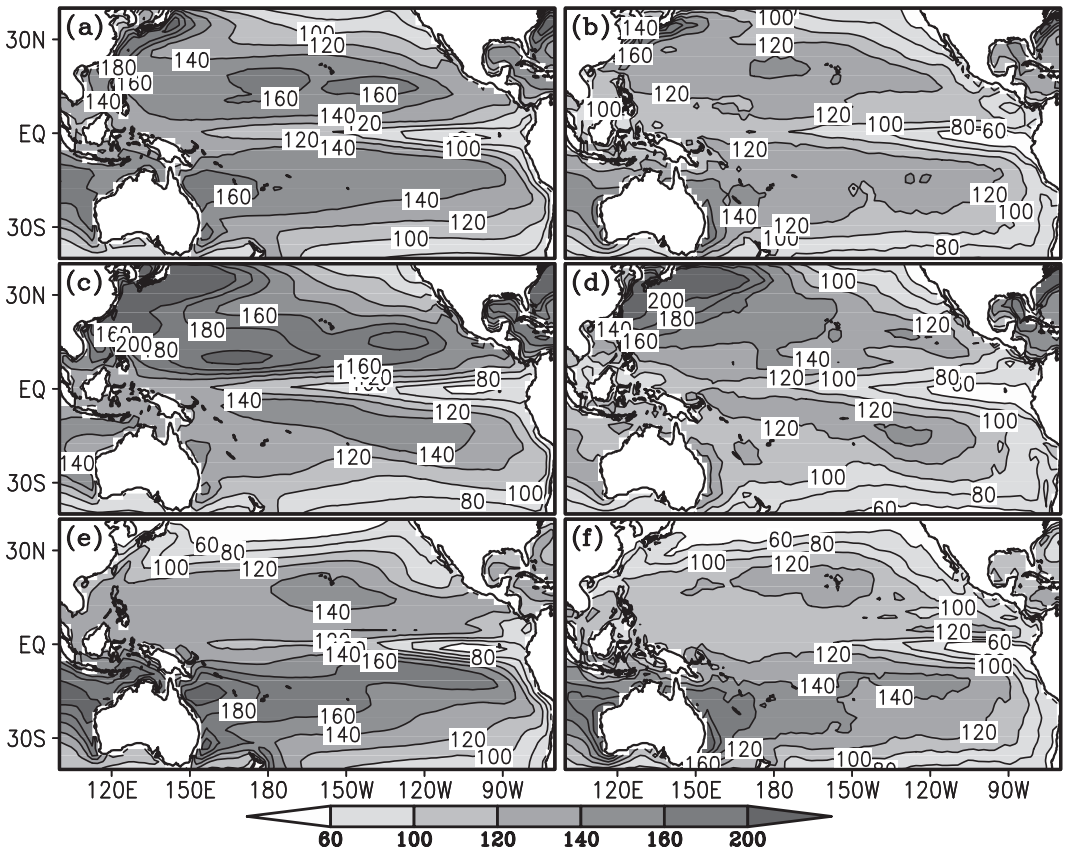

Fig. 2. The climatological mean state of LHF (units: W m^{-2}) over the TSP. The MME-mean distributions are shown in the left panels for the (a) annual average, (c) northern winter average (DJF), and (e) austral winter average (JJA). Observations from the OAFlux data are shown in the right panels for the (b) annual average, (d) northern winter average (DJF), and (f) austral winter average (JJA). The averages are constructed from the 1979–2005 base period.

correlations of LHF all lie between 0.80 and 0.90, with an average of 0.84, while the spatial variations are all larger than the observed, except FGOALS-s2 (0.97). Since the pattern correlations are not very different from each other, the centered RMSEs of the models are mainly caused by the relatively large spatial variations. Accordingly, the three best performing models are CESM1-CAM5, CNRM-CM5 and FGOALS-s2, while the poorest performing models are GFDL-ESM2M, MIROC-ESM and the MME mean. The model-simulated patterns of SST and near-surface atmospheric specific humidity mean fields all agree well with observations, with large pattern correlations of greater than 0.96 and small centered RMSEs below 0.5. However, the spatial variations of atmospheric specific humidity are generally smaller than the observations, while those of SST are all very close to observations. Additionally, the near-surface wind speed climatology in the model simulations do not agree very well with observations, and the 14 models can be split into two distinct groups: one with relatively high correlations and low variations (group 1: BCC-CSM1.1, CanESM2, CESM1-CAM5, GISS-E2-R, HadCM3, IPSL-CM5A-LR, and the MME mean); and the other with relatively low correlations and high variations (group 2: CNRM-CM5, CSIRO-Mk3.6.0, FGOALS-s2, GFDL-ESM2M, IMN-CM4, MIROC-ESM, MRI-CGCM3, NorESM1-M). Near-surface wind speeds simulated by the models, except FGOALS-s2, in group 2, are all computed from the eastward and northward near-surface wind component, but the near-surface wind speeds of the models in group 1 are directly from the outputs of the model runs. The differences between the two groups may lie in the methods of data access. Given the sampling frequency of data used in this paper is monthly, the monthly mean of the wind speed will surely be larger than the square root of the monthly mean zonal and meridional wind components, because these components may fall in different directions during a sample month. Thus, the only models that can be evaluated as near-surface wind speed driving the LHF are the six models in group 1 and FGOALS-s2 in group 2. The pattern correlations of the six models in group 1 all lie between 0.84 and 0.90, with an average of 0.86, while for FGOALS-s2 the value is 0.50. The spatial variations of the group 1 models are all larger than observed, except for CESM1-CAM5 (0.95). The RMSEs show that all six models in group 1 agree well with observations, with RMSEs below 1, but FGOALS-s2 does not agree very well with observations in its simulation of near-surface wind speed. For the

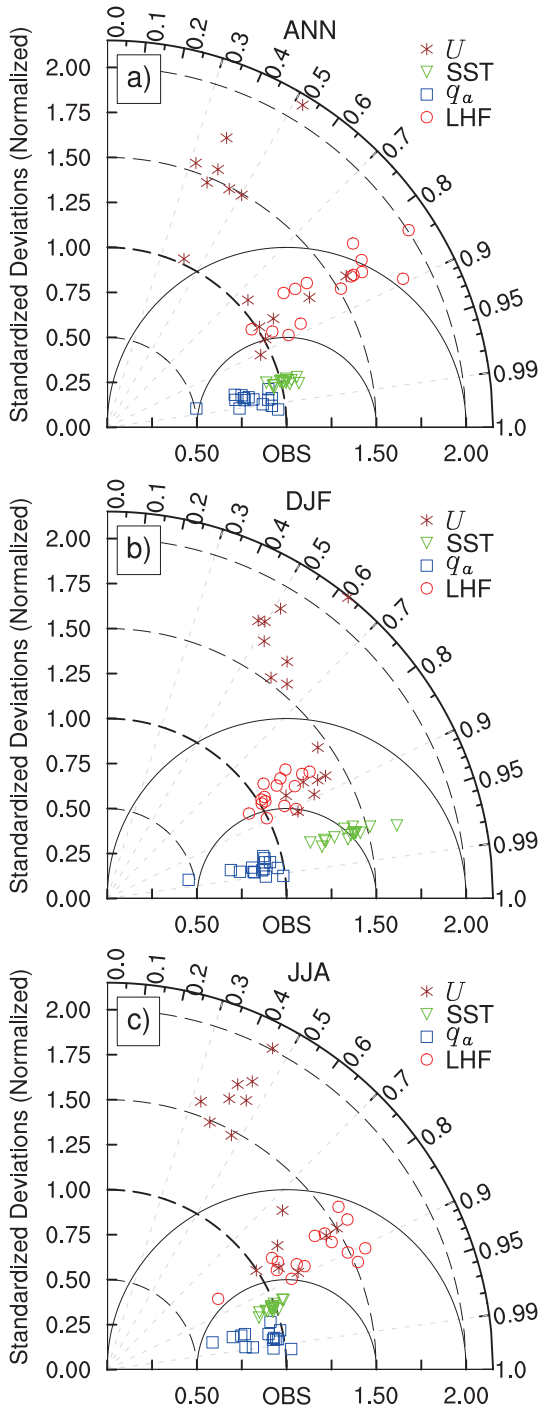

Fig. 3. Taylor diagrams for evaluating how the models reproduce the climatological mean state of LHF and related state variables including near-surface wind speed (U), SST and near-surface atmospheric specific humidity (q_a), against OAFlux data, using 14 CMIP5 models and the MME mean, for the (a) annual average, (b) northern winter average (DJF), and (c) austral winter average (JJA). The averages are constructed from the 1979–2005 base period. The angular distance from the x-axis denotes the spatial correlation coefficient between each model output and the observation. That is, the distance between each simulation and the observation quantifies the accuracy of LHF, SST, q_a and U simulated by the models against observational data.

boreal winter (DJF mean) in Fig. 3b and boreal summer (JJA mean) in Fig. 3c, the results are similar to those described above. The differences in pattern correlations of LHF, SST, atmospheric specific humidity, and group 1 models' near-surface wind speed between Fig. 3a and Fig. 3b are quite small. However, in Fig. 3b the spatial variations of LHF are much more concentrated and closer to the observations, while the variations of SST are much larger.

From Eq. (1) we know that the surface LHF can be determined from the state variables of near-surface wind, SST and atmospheric specific humidity, in which the near-surface wind and SST provide positive feedback while the atmospheric specific humidity provides negative feedback. In Fig. 3, the distributions of pattern correlations and spatial variations of simulated LHF and near-surface wind speed are well matched, despite the poor performing models whose near-surface wind speeds are computed by the zonal and meridional wind components. This indicates that the biases of the CMIP5 models in simulating the LHF mean fields may derive from biases of near-surface wind speed simulations. In Figs. 3a and c, the spatial variations of LHF and near-surface wind speed are generally larger than observed, and those of SST have the same standard deviations as the observed. Comparing Figs. 3a and b, or Figs. 3b and c, when the spatial variations of near-surface wind speed and atmospheric specific humidity differ negligibly, the SST provides positive feedback, offsetting the negative feedback of the atmospheric specific humidity on the LHF.

3.2. *Inter-model diversity*

The inter-model variability of annual mean LHF climatology over the TSP is examined by performing an inter-model EOF analysis. Figure 4 presents the result of the EOF analysis, in which the normalized first two patterns and corresponding principal components (PCs) are shown. The first mode (EOF1 in Fig. 4a, explaining 33.5% of the total variance) exhibits a broad pattern of positive LHF anomalies over the entire TSP, with maximums mainly covering the equatorial and subtropical Pacific and the strong western boundary current, especially in the Kuroshio Current region, Indonesia, and the Gulf of Mexico. The first principal component (PC1) is highly correlated (0.99) to the area-averaged LHF over the TSP (Fig. 4c). Combining the first EOF and models' PCs, there are some models showing positive LHF anomalies and others showing negative LHF anomalies. The three most positive models are FGOALS-s2, GISS-E2-R and IMN-CM4, and the three most negative models are MIROC-ESM, NorESM1-M and IPSL-CM5A-LR. The second mode, explaining 14.8% of the total variance, features a sharp positive peak over the central equatorial Pacific, and positive anomalies also occur over the eastern subtropical Pacific in both hemispheres, but relatively negative anomalies cover all other regions and peak on both sides of the equator, over Indonesia, and the Gulf of Mexico. The PC2s of the models in Fig. 4d show that the models of highest PC2 values are classified as strong central equatorial latent heat release models (first three: NorESM1-M, CESM1-CAM5, CNRM-

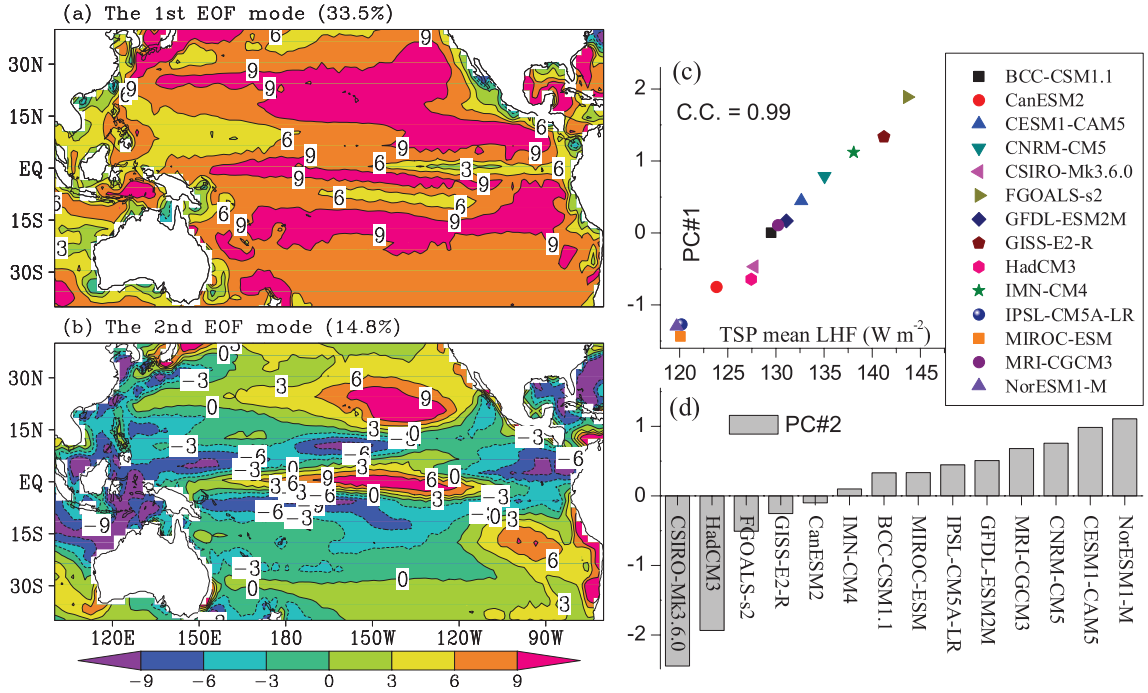

Fig. 4. The inter-model EOF analysis of 14 CMIP5 model simulations of the climatological LHF mean state: (a, b) the first and second modes of EOF spatial patterns; (c) the first PC of models correlating to regional-mean LHF climatology; (d) the second PC of models, sorted in ascending order.

CM5), while models of lowest PC2 values are classified as weak central equatorial latent heat release models (first three: CSIRO-Mk3.6.0, HadCM3, FGOALS-s2).

To examine the sources of inter-model diversity in simulating LHF climatology based on CMIP5, the LHF and related state variables of near-surface wind, SST and atmospheric specific humidity are regressed on the models' PC1s and PC2s, and the meridional profiles of the zonal mean (100°E–70°W) of these regressed variables are shown in Fig. 5. From Fig. 5a, the PC1-regressed LHF shows a well-balanced positive zonal-mean distribution along the meridian that can be seen in Fig. 4a. Over 20°–40°N and 20°–40°S, the LHF is determined by the negative atmospheric specific humidity, surface wind speed, and positive SST, but over 20°N–20°S the variability of LHF is mainly caused by the meridional variability of positive SST and negative atmospheric specific humidity, because the wind speed changes little and is close to zero in this meridional range. In Fig. 5b, the PC2-regressed LHF has very large variations along the meridian, with four positive peaks at 30°S, 0°, 25°N and 40°N, and two significant negative valleys at about 5°S and 5°N. Another valley lies at 30°N, with a value close to zero. The peaks at 30°S, 0°, 25°N and 40°N correspond respectively to the positive anomalies in Fig. 4b, and the valleys correspond to the negative anomalies. From this figure, the LHF is highly correlated with SST and less correlated with atmospheric specific humidity between 20°N and 20°S, while over 20°–40°N and 20°–40°S the LHF is more correlated to the surface wind speed. These results are very similar to those shown in Fig. 5a.

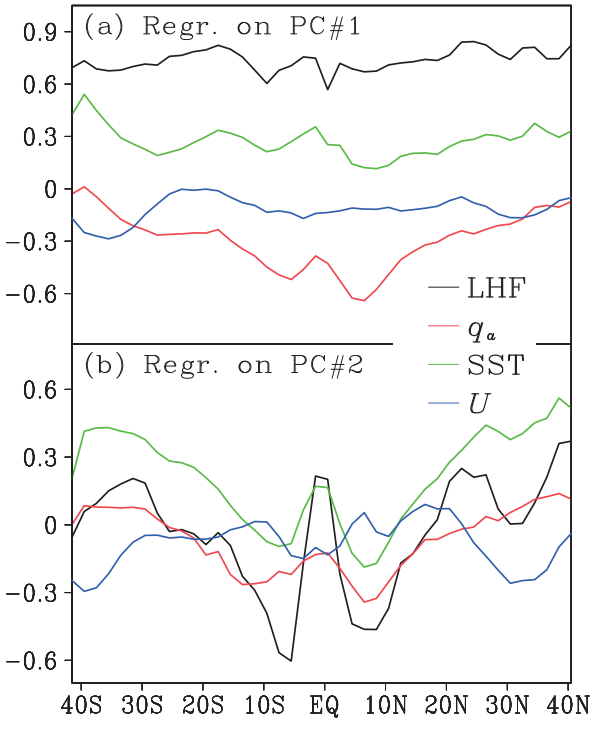

Fig. 5. Meridional profiles of zonal-mean (100°E–70°W) climatological LHF (units: 10 W m^{-2}) and related state variables including near-surface wind speed (U; units: m s^{-1}), SST (units: °C) and near-surface atmospheric specific humidity (q_a; units: g kg^{-1}), regressed on (a) the first PCs of models and (b) the second PCs of models in Fig. 4.

3.3. *Climatological seasonal variation*

In climatology, seasonal variation is the part of a measured quantity's fluctuation that is attributed to Earth's changing position in orbit over the course of the year. Figure 6 shows the time–latitude sections of zonal mean (100°E–70°W) climatological LHF and related state variables of atmospheric specific humidity, SST and near-surface wind during 1979–2005. Compared to the LHF observations from OAFlux (Fig. 6a1), the agreement of the MME mean (Fig. 6a2) is very good over most of the year. In particular, the MME mean reproduces the maximum over the southern subtropical Pacific in June to August, and over the northern subtropical Pacific in December to February. This is a fairly realistic position change of the latent heat release center over the course of the year. Over the tropics, LHF overestimations of around 20 W m^{-2} are apparent through the year in the MME compared to the observations (see Fig. 6a3). As with the LHF, the comparisons of the related state variables of atmospheric specific humidity, SST and near-surface wind are shown in Figs. 6b–d. The mean simulations of atmospheric specific humidity and SST are both in good agreement with observations, throughout the year, tracing a significant change of solar orbit position, and the maximum being located on both sides of the equator. The atmospheric specific humidity bias is about 1 g kg^{-1} over the entire meridional range in this figure. The biases of SST are mainly located in the latitudes of 20°–40°N and 20°–40°S. Comparing the surface wind speed of the MME mean and observations in Fig. 6d, the changing pattern over the course of the year and the maxima and minima all match well. However, there are relatively large biases during June to December (i.e., the latter half of the year) over the entire meridional range in this figure, and the biases of the first half of the year mainly occur over the Northern Hemisphere.

Since the seasonal variations are highly correlated to the changing subsolar point, the features of seasonal variation in the Northern Hemisphere and Southern Hemisphere should be very different. Figure 7 presents the pattern statistics describing the climatological seasonal variation of LHF and related state variables (near-surface wind speed, SST and near-surface atmospheric specific humidity), just like in Fig. 3, over the northern TSP (100°E–70°W, 0°–40°N) and southern TSP (100°E–70°W, 0°–40°S), simulated by the 14 CMIP5 models and MME mean, compared with the observed (OAFlux). Over both the northern and southern TSP, the pattern correlations of the climatological seasonal variation of LHF, SST and atmospheric specific humidity all exceed the 99.9% confidence level, with distribution-intensive standard variations nearer 1 and relatively low centered RMSEs. The biases of near-surface wind speed again show large RMSEs and relatively low correlations. The most mismatched

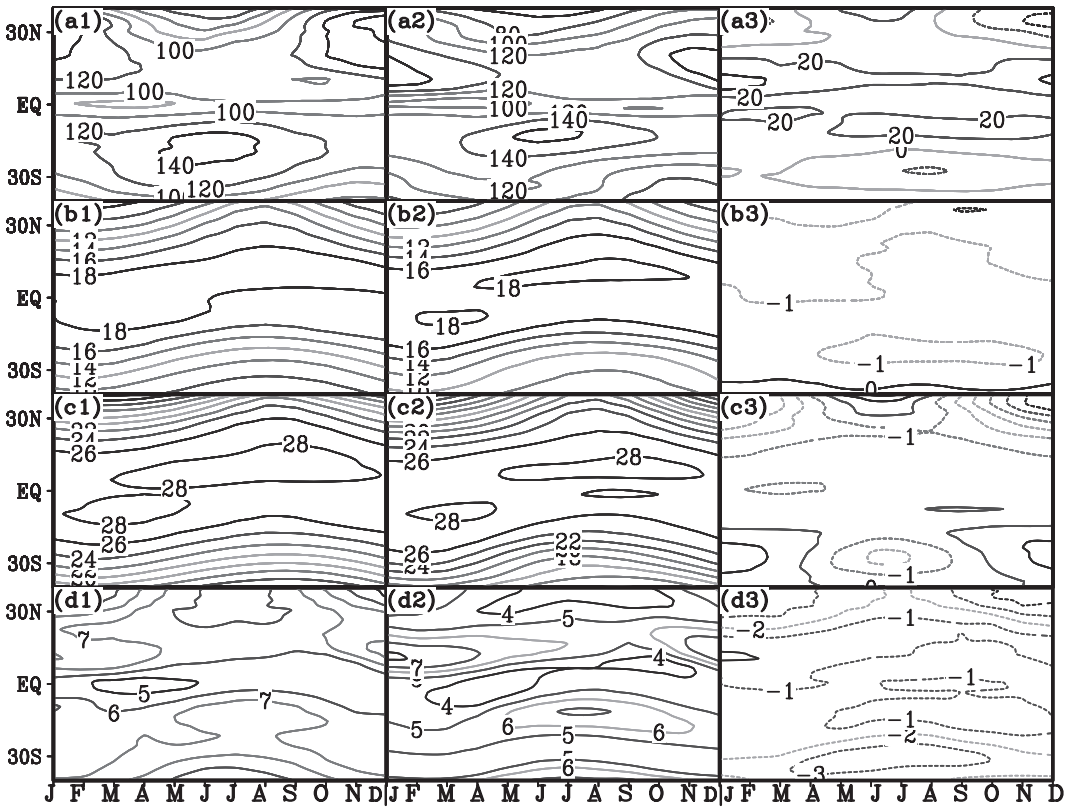

Fig. 6. (a) Time–latitude sections of the zonal-mean (100°E–70°W) climatological LHF (W m^{-2}) from (a1) OAFlux data, (a2) the MME mean, and (a3) the differences between the two (MME minus OAFlux). The same is also shown for (b1–b3) near-surface atmospheric specific humidity (units: g kg^{-1}), (c1–c3) SST (units: °C), and (d1–d3) near-surface wind speed (units: m s^{-1}).

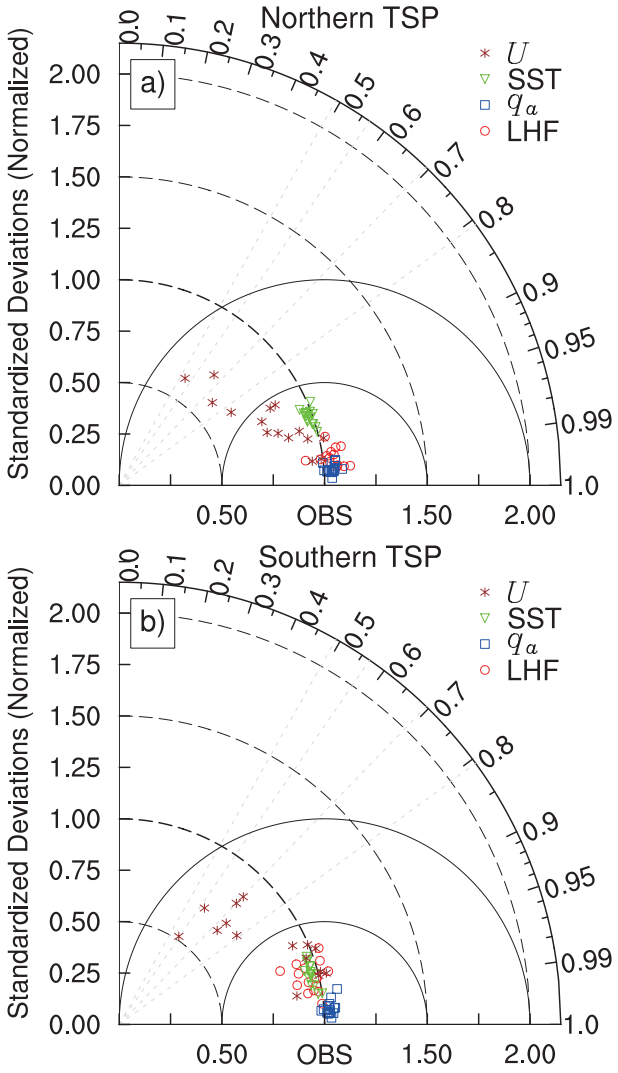

Fig. 7. Pattern statistics describing the climatological seasonal variation of LHF and related state variables including near-surface wind speed (U), SST and near-surface atmospheric specific humidity (q_a), over the northern TSP (0°–40°N, 100°E–70°W) and southern TSP (0°–40°S, 100°E–70°W), simulated by 14 CMIP5 models and the MME mean, compared with observation (OAFlux).

models, whose wind speeds' seasonal variation correlations to observations do not exceed the 99.9% confidence level, are FGOALS-s2, CSIRO-Mk3.6.0 and MIROC-ESM in the northern TSP, and in the southern TSP they are CNRM-CM5, CSIRO-Mk3.6.0, FGOALS-s2, GFDL-ESM2M, MIROC-ESM, MRI-CGCM3 and NorESM1-M. These are all group 2 models (see section 3.1 and Fig. 3). As explained in section 3.1, except FGOALS-s2, the errors of the surface wind speed simulations of the models not exceeding the 99.9% confidence level may come from the computing of monthly surface wind speed from the monthly mean zonal and meridional wind components. Nevertheless, there are five group 2 models that simulate the northern TSP wind speed seasonal variation in good agreement with observations, with correlations exceeding the 99.9% confidence level; while in the southern TSP, there is only one group 2 model (INM-CM4) exceeding this level. This result is consistent with the bias distribution differences between the northern and southern TSP in Fig. 6d.

3.4. *Long-term upward trend*

Whether from global warming forcing or the dynamics of climate oscillation, trends are very important in climate research and are ubiquitous in the climate system. Although the climate variability in a fully coupled model is produced by itself and has nothing to do with the observed climate variability, the climate trend responding to the increase of CO_2 designated in CGCMs can be evaluated for improving climate prediction and diagnosis using models.

Since the distinct transition from a downward trend to an upward trend around 1977–78 (Yu, 2007), the LHF has been rising continuously. Figure 8 presents the observed linear trend distributions and yearly mean variations averaged over the TSP for LHF, near-surface atmospheric specific humidity, SST, and near-surface wind speed. The results of the MME mean are shown in Fig. 9. For the observed LHF in Fig. 8a, a large-scale positive trend structure is captured along the western boundary current, especially over the Kuroshio Current and its extension and the equatorial central-western Pacific. Meanwhile, a negative trend exists in the equatorial eastern Pacific and in the subtropical eastern Pacific in both hemispheres. The trend patterns of near-surface atmospheric specific humidity (Fig. 8c) and SST (Fig. 8e) both show La Niña–like conditions. The positive feedback of the SST trend is much larger than the negative feedback of the near-surface atmospheric specific humidity, so the trend pattern of LHF coincides with the SST trend. The trend of near-surface wind speed, whose maxima and minima match well with those of LHF, is shown in Fig. 8g. The 1979–2005 annual mean variabilities of LHF, atmospheric specific humidity, SST and near-surface wind speed in Figs. 8b, d, f and h are highly correlated with a significant trend. In Fig. 9, for the MME mean, the pattern of the LHF trend does not match the observations. To identify the origins of the biases, the atmospheric specific humidity, SST and near-surface wind speed trends are shown in Figs. 9c, e and g. The atmospheric specific humidity and SST trend patterns show an overall positive trend over the TSP. The atmospheric specific humidity trend shows maxima over the equatorial regions, with significant poleward decreasing gradients, but there are no significant east–west gradients. The trend pattern of SST peaks over the northern TSP and a positive trend is distributed uniformly over the central-western Pacific. North–south gradients are located in the eastern Pacific, and there are east–west gradients in the southern TSP. All these gradients derive from the relatively lower trend over the regions off the west coast of South America. There is no significant near-surface wind speed trend that can be captured by Fig. 9g, except a very small positive trend over the southeastern TSP. The 1979–2005 annual mean variabilities of LHF, atmospheric specific humidity and SST show significant trends, but not for near-surface wind speed.

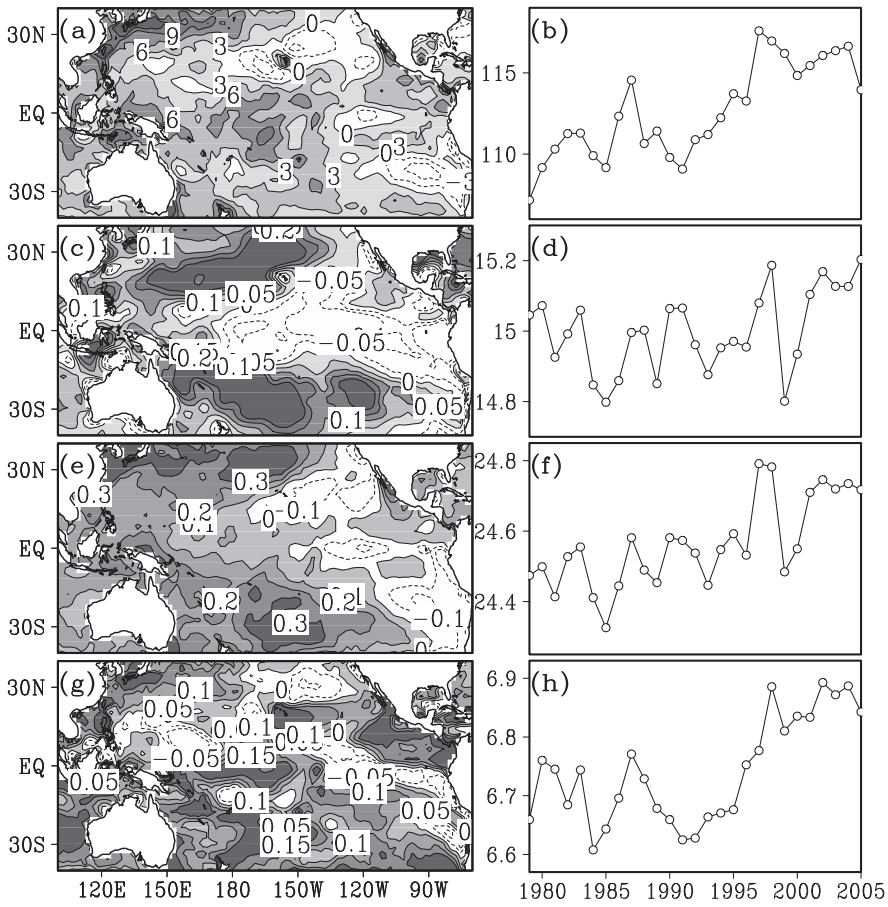

Fig. 8. The observed linear trend $(10\ \mathrm{yr})^{-1}$ distributions and yearly mean variations averaged over the TSP of (a, b) LHF (units: W m^{-2}), (c, d) near-surface atmospheric specific humidity (units: g kg^{-1}), (e, f) SST (units: °C), and (g, h) near-surface wind speed (units: m s^{-1}), using OAFlux data.

Using linear least-squares fitting, the decadal trends of annual mean LHF and related state variables (atmospheric specific humidity, SST and near-surface wind speed) averaged over the TSP using the 14 CMIP5 CGCMs, the MME mean and observations (OAFlux data) are computed and shown in Table 2. The observed trends of LHF and related state variables all exceed the 95% confidence level, using the method of Santer et al. (2000), after taking into account the autocorrelation of the noise in the data. From Table 2, there are only two models (BCC-CSM1.1 and IPSL-CM5A-LR) whose LHF trend exceeds the 95% confidence level, with values of 0.53 ± 0.51 and 1.31 ± 0.41 W m^{-2} $(10\ \mathrm{yr})^{-1}$, respectively. However, these are much lower than the observed values of 2.96 ± 0.95 W m^{-2} $(10\ \mathrm{yr})^{-1}$. Thus, the MME mean is just able to exceed the 95% confidence level, with a very small trend of 0.37 ± 0.23 W m^{-2} $(10\ \mathrm{yr})^{-1}$. The trends of atmospheric specific humidity and SST in all 14 models and the MME mean exceed the 95% confidence level, indicating that the CMIP5 CGCMs simulate significant increasing trends of near-surface atmospheric specific humidity and SST. The biggest and smallest trends of atmospheric specific humidity and SST are captured by IPSL-CM5A-LR and INM-CM4, which are 0.32 ± 0.07 g kg^{-1} $(10\ \mathrm{yr})^{-1}$, 0.32 ± 0.07 °C $(10\ \mathrm{yr})^{-1}$, and 0.07 ± 0.04 g kg^{-1} $(10\ \mathrm{yr})^{-1}$, 0.06 ± 0.05°C $(10\ \mathrm{yr})^{-1}$, respectively. The MME-mean atmospheric specific humidity and SST trends are 0.16 ± 0.06 g kg^{-1} $(10\ \mathrm{yr})^{-1}$ and 0.15 ± 0.06°C $(10\ \mathrm{yr})^{-1}$. Obviously, even the smallest trends of model-simulated atmospheric specific humidity and SST are bigger than observed. This means that the trends of atmospheric specific humidity and SST are grossly overestimated by the CMIP5 CGCMs. Because the atmospheric specific humidity and SST feedbacks on the LHF are opposite, the trend feedback of Δq in Eq. (1) will be very weak in cases where the difference between the positive feedback of SST and the negative feedback of atmospheric specific humidity is minimal. The trends of near-surface wind speed in Table 2 show that there is no model-simulated trend of near-surface wind speed exceeding the 95% confidence level.

4. Summary and discussion

4.1. *Summary*

Based on the OAFlux dataset (verified using NOCS V2 flux data) and the historical-scenario simulations from 14

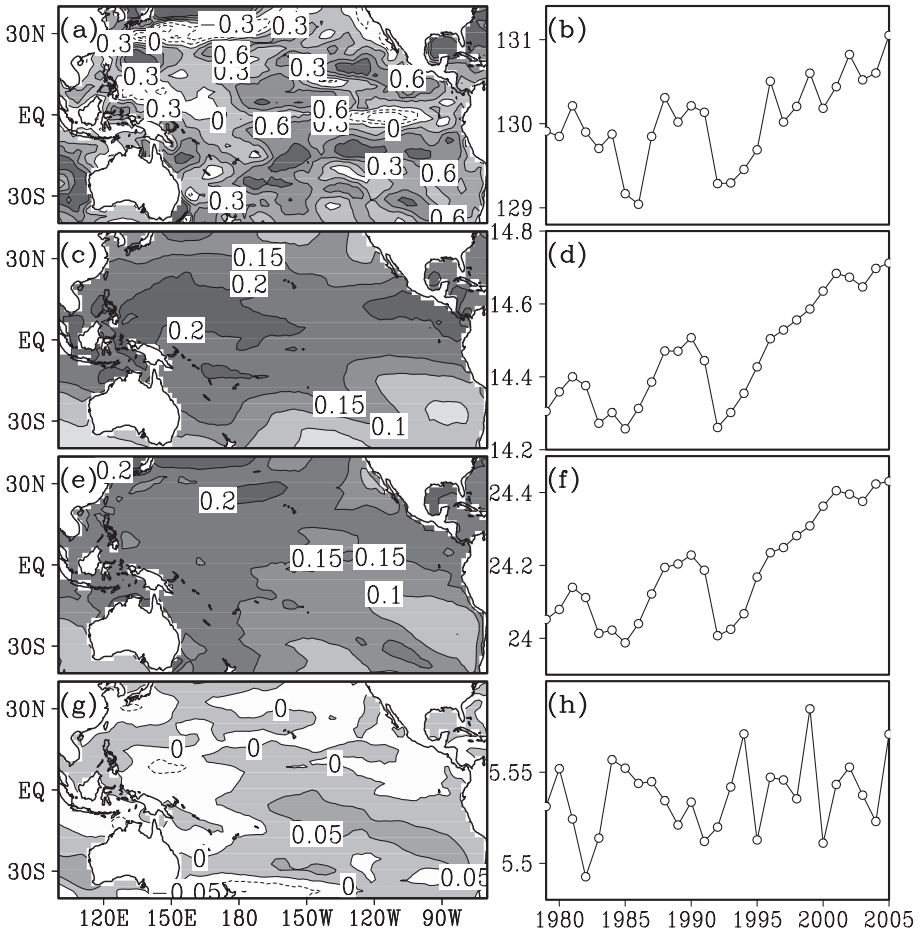

Fig. 9. As in Fig. 8 but for the MME mean.

Table 2. The linear trends and 95% confidence intervals of model-simulated annual LHF and related state variables averaged over the TSP for the 14 CMIP5 models and MME mean compared with observations from OAFlux data*.

	Linear Trend and 95% confidence interval $(10\ \text{yr})^{-1}$			
	LHF (W m^{-2})	Atmospheric specific humidity (g kg^{-1})	SST (°C)	Near-surface wind speed (m s^{-1})
BCC-CSM1.1	**0.53 ± 0.51**	**0.18 ± 0.06**	**0.18 ± 0.06**	0.00 ± 0.03
CanESM2	0.47 ± 0.51	**0.21 ± 0.09**	**0.20 ± 0.08**	0.00 ± 0.02
CESM1-CAM5	0.08 ± 0.61	**0.11 ± 0.07**	**0.11 ± 0.08**	−0.01 ± 0.03
CNRM-CM5	0.34 ± 0.53	**0.16 ± 0.05**	**0.15 ± 0.05**	0.03 ± 0.04
CSIRO-Mk3.6.0	0.18 ± 0.50	**0.12 ± 0.08**	**0.11 ± 0.08**	0.02 ± 0.04
FGOALS-s2	0.17 ± 0.62	**0.20 ± 0.11**	**0.20 ± 0.11**	0.00 ± 0.05
GFDL-ESM2M	0.26 ± 0.89	**0.19 ± 0.08**	**0.18 ± 0.08**	0.01 ± 0.05
GISS-E2-R	0.21 ± 0.52	**0.11 ± 0.08**	**0.10 ± 0.09**	0.00 ± 0.02
HadCM3	0.63 ± 0.66	**0.20 ± 0.10**	**0.21 ± 0.11**	−0.01 ± 0.03
INM-CM4	0.10 ± 0.27	**0.07 ± 0.04**	**0.06 ± 0.05**	0.01 ± 0.03
IPSL-CM5A-LR	**1.31 ± 0.41**	**0.32 ± 0.07**	**0.32 ± 0.07**	−0.01 ± 0.02
MIROC-ESM	0.31 ± 0.44	**0.11 ± 0.08**	**0.10 ± 0.07**	0.03 ± 0.05
MRI-CGCM3	0.29 ± 0.39	**0.09 ± 0.04**	**0.08 ± 0.03**	−0.01 ± 0.04
NorESM1-M	0.32 ± 0.64	**0.12 ± 0.06**	**0.11 ± 0.06**	0.03 ± 0.04
MME mean	**0.37 ± 0.23**	**0.16 ± 0.06**	**0.15 ± 0.06**	0.01 ± 0.01
OBS(OAFlux)	**2.96 ± 0.95**	**0.06 ± 0.06**	**0.11 ± 0.05**	**0.08 ± 0.04**

*Boldface indicates the linear trend exceeds the 95% confidence level, using the method of Santer et al. (2000), after taking into account the autocorrelation of the noise in the data.

CMIP5 CGCMs, the LHF over the TSP and the origins of simulation biases have been diagnosed and systematically assessed in this study. From discussion of the climatological mean fields, inter-model variability, climatological seasonal variation, and long-term trend, the main conclusions can be summarized as follows:

(1) The simulated annual-mean and seasonal-mean LHF climatology in most of the CGCMs agrees very well with the observations from OAFlux. From the comparison of the MME mean with observations, the agreement in terms of the strong and weak latent heat release centers is very good. However, the models simulate stronger LHF over most of the TSP. The differences between the CMIP5 outputs and OAFlux can be as large as 20–30 W m^{-2} in the subtropical oceans. Pattern statistics describing the annual- and seasonal-mean LHF climatology and related state variables show that the biases of near-surface wind speed may be the origin of the LHF biases in the CMIP5 models. Seasonal-mean differences show that SST biases and atmospheric specific humidity biases have opposite feedback effects on LHF biases.

(2) The inter-model variability of the annual-mean LHF climatology over the TSP was examined by performing an inter-model EOF analysis for the 14 CMIP5 CGCMs. The first mode indicates overall positive anomalies, reflecting the fact that models with positive PCs simulate relatively strong LHF, while models with negative PCs simulate relatively weak LHF. The first PC of the models is highly correlated with the TSP mean LHF climatology, indicating that the overall stronger or weaker LHF over the TSP, especially on the equator and in the subtropics, is the most notable diversity of the CMIP5 models. The second mode shows very large variations along the meridian. Both PC1- and PC2-regressed LHF, SST and atmospheric specific humidity have similar meridional distributions. However, the variability of near-surface wind speed has no significant relationship with LHF. This indicates that the inter-model diversity in the CMIP5 models may come from the diversity in simulating SST and near-surface atmospheric specific humidity.

(3) The agreement of the MME mean climatological seasonal variation with OAFlux is very good over most of the year. Over the tropics, LHF overestimations of around 20 W m^{-2} are apparent in the MME, compared to observations. The mean simulations of atmospheric specific humidity and SST are both in good agreement with observations, throughout the year, tracing a significant changing solar orbit position, and the maximum is located on both sides of the equator. Pattern statistics describing the climatological seasonal variation of LHF and related state variables over the northern and southern TSP, simulated by the 14 CMIP5 models and the MME mean, compared with the observed (OAFlux), show that–over both the northern and southern TSP–the pattern correlations of LHF, SST and atmospheric specific humidity all exceed the 99.9% confidence level. The errors in the models' simulations of near-surface wind speed not exceeding the 99.9% confidence level may derive from the computing of monthly surface wind speed from the monthly mean zonal and meridional wind components.

(4) The linear trend pattern of LHF in the MME mean does not match the observations well. The observed trends of LHF and related state variables all exceed the 95% confidence level. Few models (only two) simulate the LHF and near-surface wind speed trends exceeding the 95% confidence level. The trends of atmospheric specific humidity and SST in all 14 models and the MME mean exceed the 95% confidence level, indicating that the CMIP5 CGCMs simulate significant increasing trends of near-surface atmospheric specific humidity and SST. The trends of atmospheric specific humidity and SST are grossly overestimated by the CMIP5 CGCMs, while the trends of LHF and near-surface wind speed are largely underestimated. So, the feedback effects of the atmospheric specific humidity and SST trends are both overestimated by the models, and the trend feedback of specific humidity differences will be very weak in cases where the difference between the positive feedback of the SST and negative feedback of atmospheric specific humidity is minimal.

4.2. *Discussion*

LHF serves energy to the evaporation process, which is important in the global water cycle. The bulk aerodynamic formula tells us that recent changes of LHF are likely related to changes in surface winds, SST and near-surface atmospheric specific humidity. For climatology, model-simulated biases of surface LHF may come from the offset errors of near-surface wind speed in CMIP5 MMEs. Inter-model EOF analysis indicates the model diversity in simulating LHF may come from the diversity in simulating the state variables of SST and near-surface atmospheric specific humidity (temperature differences or specific humidity differences). The climatological seasonal variation in CMIP5 models is different in the North and South Pacific, but the biases against observation both generally originate from the wind speed biases. For trend analysis, the poor abilities of models to reproduce the observed LHF long-term trend may intuitively be a result of the overestimation of SST and atmospheric specific humidity, but essentially may be a result of many natural and model-associated stochastic factors acting together, which still needs to be studied.

Many of these biases can be substantially reduced using bias-correction procedures, which could make these runs useful for climate change studies (Maurer and Hidalgo, 2008; Maurer et al., 2010). However, while the bias will be reduced, the variance will also be increased. So, for it to be useful, the improvement in bias must be large relative to the loss in variance. Thus, using CMIP5 multi-model projections of the climatological mean state and seasonal variation of LHF in future research on the hydrological cycle and heat transport could lead to relatively good results, despite some regional variances. However, for trend projections of LHF, the trend rates and trend patterns require careful consideration. The distributions of the LHF trend pattern are not very credible. Better simulations of identified tropical and subtropical circulation processes will improve simulations of the LHF trend, which is a potential area of future research.

Acknowledgements. The authors would like to thank the two anonymous reviewers for their valuable comments which led to a significant improvement of the manuscript. This research was supported by the National Basic Research Program of China (Grant No. 2012CB417403), the Strategic Priority Research Program of the Chinese Academy of Sciences (Grant No. XDA05090402), and the Opening Project of Key Laboratory of Meteorological Disaster of Ministry of Education of Nanjing University of Information Science and Technology (Grant No. KLME1401). The authors also acknowledge the use of the CMIP5 datasets, OAFlux products and NOC surface flux dataset.

REFERENCES

Alexander, M. A., and J. D. Scott, 1997: Surface flux variability over the North Pacific and North Atlantic Oceans. *J. Climate*, **10**, 2963–2978.

Berry, D. I., and E. C. Kent, 2009: A new air-sea interaction gridded dataset from ICOADS with uncertainty estimates. *Bull. Amer. Meteor. Soc*., **90**, 645–656.

Berry, D. I., and E. C. Kent, 2011: Air-sea fluxes from ICOADS: The construction of a new gridded dataset with uncertainty estimates. *Inter. J Climatol.*, **31**, 987–1001.

Bigg, G. R., T. D. Jickells, P. S. Liss, and T. J. Osborn, 2003: The role of the oceans in climate. *Int. J. Climatol.*, **23**, 1127–1159, doi: 10.1002/joc.926.

Burgman, R. J., A. C. Clement, C. M. Mitas, J. Chen, and K. Esslinger, 2008: Evidence for atmospheric variability over the Pacific on decadal timescales. *Geophys. Res. Lett.*, **35**(1), L01704, doi: 10.1029/2007GL031830.

Cayan, D. R., 1992a: Variability of latent and sensible heat fluxes estimated using bulk formulae. *Atmos.-Ocean*, **30**, 1–42.

Cayan, D. R., 1992b: Latent and sensible heat flux anomalies over the northern oceans: The connection to monthly atmospheric circulation. *J. Climate*, **5**, 354–369.

Cayan, D. R., 1992c: Latent and sensible heat flux anomalies over the northern oceans: Driving the sea surface temperature. *J. Phys. Oceanogr.*, **22**, 859–881.

Chen, J. Y., B. E. Carlson, and A. D. Del Genio, 2002: Evidence for strengthening of the tropical general circulation in the 1990s. *Science*, **295**, 838–841.

Fairall, C. W., E. F. Bradley, J. E. Hare, A. A. Grachev, and J. B. Edson, 2003: Bulk parameterization of air-sea fluxes: updates and verification for the COARE algorithm. *J. Climate*, **16**, 571–591.

Grodsky, S. A., A. Bentamy, J. A. Carton, and R. T. Pinker, 2009: Intraseasonal latent heat flux based on satellite observations. *J. Climate*, **22**, 4539–4556.

Gulev, S. K., 1995: Long-term variability of sea-air heat transfer in the North Atlantic Ocean. *Inter. J. Climatol.*, **15**, 825–852, doi: 10.1002/joc.3370150802.

Hayashi, Y., 1982: Confidence intervals of a climatic signal. *J. Atmos. Sci.*, **39**, 1895–1905.

Held, I. M., and B. J. Soden, 2006: Robust responses of the hydrological cycle to global warming. *J. Climate*, **19**(21), 5686–5699.

Kiehl, J. T., and K. E. Trenberth, 1997: Earth's annual global mean energy budget. *Bull. Amer. Meteor. Soc.*, **78**, 197–208.

Li, G., B. H. Ren, C. Y. Yang, and J. Q. Zheng, 2011a: Revisiting the trend of the tropical and subtropical Pacific surface latent heat flux during 1977–2006. *J. Geophys. Res.*, **116**, D10115, doi: 10.1029/2010JD015444.

Li, G., B. H. Ren, J. Q. Zheng, and C. Y. Yang, 2011b: Net air-sea surface heat flux during 1984–2004 over the North Pacific and North Atlantic oceans (10°N–50°N): Annual mean climatology and trend. *Theor. Appl. Climatol.*, **104**, 387–401.

Li, G., and S. P. Xie, 2012: Origins of tropical-wide SST biases in CMIP multi-model ensembles. *Geophys. Res. Lett.*, **39**(22), L22703, doi: 10.1029/2012GL053777.

Liu, J. P., and J. A. Curry, 2006: Variability of the tropical and subtropical ocean surface latent heat flux during 1989–2000. *Geophys. Res. Lett.*, **33**, L05706, doi: 10.1029/2005GL024809.

Liu, W. T., K. B. Katsaros, and J. A. Businger, 1979: Bulk parameterizations of air-sea exchanges of heat and water vapor including the molecular constraints at the interface. *J. Atmos. Sci.*, **36**, 1722–1735.

Maurer, E. P., and H. G. Hidalgo, 2008: Utility of daily vs. monthly large-scale climate data: an intercomparison of two statistical downscaling methods. *Hydrology and Earth System Sciences*, **12**, 551–563.

Maurer, E. P., L. D. Brekke, and T. Pruitt, 2010: Contrasting lumped and distributed hydrology models for estimating climate change impacts on California watersheds. *Journal of the American Water Resources Association*, **46**(5), 1024–1035.

Meehl, G. A., G. J. Boer, C. Covey, M. Latif, and R. J. Stouffer, 1997: Intercomparison makes for a better climate model. *Eos, Trans. Amer. Geophys. Union*, **78**(41), 445–451.

Meehl, G. A., G. J. Boer, C. Covey, M. Latif, and R. J. Stouffer, 2000: The coupled model intercomparison project (CMIP). *Bull. Amer. Meteor. Soc.*, **81**(2), 313–318.

Mitas, C. M., and A. Clement, 2006: Recent behavior of the Hadley cell and tropical thermodynamics in climate models and reanalyses. *Geophys. Res. Lett.*, **33**(1), L01810, doi: 10.1029/2005GL024406.

O'Brien, E. W., and F. Horsfall, 1995: Sensitivity of the heat budget in a midlatitude ocean model to variations in atmospheric forcing. *J. Geophys. Res.*, **100**, 24 761–24 772.

Papadopoulos, V. P., Y. Abualnaja, S. A. Josey, A. Bower, D. E. Raitsos, H. Kontoyiannis, and I. Hoteit, 2013: Atmospheric forcing of the winter air-sea heat fluxes over the Northern Red Sea. *J. Climate*, **26**, 1685–1701.

Quan, X. W., H. F. Diaz, and M. P. Hoerling, 2004: Change in the tropical Hadley cell since 1950. *The Hadley Circulation: Present, Past, and Future*, Diaz and Bradley, Eds., Springer Netherlands, 85–120.

Reichler, T., and J. Kim, 2008: How well do coupled models simulate today's climate. *Bull. Amer. Meteor. Soc.*, **89**(3), 303–311.

Santer, B. D., T. M. L. Wigley, J. S. Boyle, D. J. Gaffen, J. J. Hnilo, D. Nychka, D. E. Parker, and K. E. Taylor, 2000: Statistical significance of trends and trend differences in layer-average atmospheric temperature time series. *J. Geophys. Res.*, **105**(D6), 7337–7356.

Taylor, K. E., 2001: Summarizing multiple aspects of model performance in a single diagram. *J. Geophys. Res.*, **106**(D7), 7183–7192.

Trenberth, K. E., 1995: Atmospheric circulation climate changes. *Climatic Change*, **31**, 427–453.

Trenberth, K. E., and A. Solomon, 1994: The global heat balance: Heat transports in the atmosphere and ocean. *Climate Dyn.*, **10**, 107–134.

Trenberth, K. E., J. T. Fasullo, and J. Kiehl, 2009: Earth's global

energy budget. *Bull. Amer. Meteor. Soc.*, **90**, 311–323.

Vecchi, G. A., and B. J. Soden, 2007: Global warming and the weakening of the tropical circulation. *J. Climate*, **20**(17), 4316–4340.

Vecchi, G. A., B. J. Soden, A. T. Wittenberg, I. M. Held, A. Leetmaa, and M. J. Harrison, 2006: Weakening of tropical Pacific atmospheric circulation due to anthropogenic forcing. *Nature*, **441**(7089), 73–76.

Wentz, F. J., L. Ricciardulli, K. Hilburn, and C. Mears, 2007: How much more rain will global warming bring? *Science*, **317**(5835), 233–235.

Yu, L. S., 2007: Global variations in oceanic evaporation (1958–2005): The role of the changing wind speed. *J. Climate*, **20**(21), 5376–5390.

Yu, L. S., and R. A. Weller, 2007: Objectively analyzed air-sea heat fluxes for the global ice-free oceans (1981–2005). *Bull. Amer. Meteor. Soc.*, **88**, 527–539.

Yu, L. S., R. A. Weller, and B. M. Sun, 2004: Mean and variability of the WHOI daily latent and sensible heat fluxes at in situ flux measurement sites in the Atlantic Ocean. *J. Climate*, **17**, 2096–2118.

Yu, L. S., X. Z. Jin, and R. A. Weller, 2007: Annual, seasonal, and interannual variability of air-sea heat fluxes in the Indian Ocean. *J. Climate*, **20**, 3190–3209.

Yu, L. S., X. Z. Jin, and R. A. Weller, 2008: Multidecade global flux datasets from the objectively analyzed air-sea fluxes (OAFlux) project: Latent and sensible heat fluxes, ocean evaporation, and related surface meteorological variables. Woods Hole Oceanographic Institution, OAFlux Project Technical Report OA-2008-01, 64 pp.

Yulaeva, E., N. Schneider, D. W. Pierce, and T. P. Barnett, 2010: Modeling of North Pacific climate variability forced by oceanic heat flux anomalies. *J. Climate*, **14**, 4027–4046.

Zhou, L. T., 2013: Influence of thermal state of warm pool in western Pacific on sensible heat flux. *Atmospheric Science Letters*, **14**, 91–96. doi: 10.1002/asl2.422

Zhou, L. T., G. S. Chen, and R. G. Wu, 2015: Change in surface latent heat flux and its association with tropical cyclone genesis in the western North Pacific. *Theor. Appl. Climatol.*, **119**, 221–227.

Zhou, Y. P., K. M. Xu, Y. C. Sud, and A. K. Betts, 2011: Recent trends of the tropical hydrological cycle inferred from Global Precipitation Climatology Project and International Satellite Cloud Climatology Project data. *J. Geophys. Res.*, **116**(D9), D09101, doi: 10.1029/2010JD015197.